John von Neumann Institute for Computing

Radiative Gas Dynamics Parallel Computing Using Unstructured Meshes

B.N. Chetverushkin, V.A. Gasilov, O.G. Olkhovskaya,
S.V. D'yachenko, E.L. Kartashova, A.S. Boldarev,
V.V. Valko

published in

Parallel Computing:
Current & Future Issues of High-End Computing,
Proceedings of the International Conference ParCo 2005,
G.R. Joubert, W.E. Nagel, F.J. Peters, O. Plata, P. Tirado, E. Zapata (Editors),
John von Neumann Institute for Computing, Jülich,
NIC Series, Vol. **33**, ISBN 3-00-017352-8, pp. 359-366, 2006.

http://www.fz-juelich.de/nic-series/volume33

Radiative gas dynamics parallel computing using unstructured meshes

B.N.Chetverushkin[a], V.A.Gasilov[a], O.G.Olkhovskaya[a], S.V.D'yachenko[a], E.L.Kartashova[a], A.S.Boldarev[a], and V.V.Valko[b]

[a]Institute for Mathematical Modelling, Russian Ac.Sci., 4-A, Miusskaya Sq., 125047, Moscow, Russia

[b]The Central Physical-Technical Institute of the RF Defence Ministry, Sergiev Posad, 141300, Moscow region, Russia

The study is supported by the State contract 10002-251/OMH-03/026-023/240603-806, ISTC project 2830, and RFBR project 04-01-08024-OFI-A.

Key words: Computational fluid dynamics; radiative transfer, unstructured mesh; parallel algorithms;

High-performance computing evidently is a proper tool for simulations of transient high-temperature flows. A lot of numerical work is typically required to resolve accurately complex multiscale nonlinear processes in hypersonic gases and plasmas. Taking this as a starting motivation we develop a new object-oriented code for simulations of coupled radiative-gasdynamics processes using unstructured grid technology. The first applications of this new code showed promising results, which make us confident in good perspectives of using the unstructured grid technologies in simulations of complex physical models. The benchmark problem presented here is the computation of hypersonic radiating flowfield over a blunt body simulating the space vehicle re-entry conditions.

1. Mathematical models and numerical methods

The code performs calculations in planar or cylindrical coordinates. We accept a single-fluid gasdynamics model including dissipative processes [1]. The gasdynamics equations are written in the form of conservation laws.

- continuity equation $\dfrac{\partial \rho}{\partial t} + \operatorname{div}(\rho \mathbf{V}) = 0$

- momentum equation $\dfrac{\partial \rho \mathbf{V}}{\partial t} + \operatorname{div}(p\mathbf{V} \otimes \mathbf{V}) = -\operatorname{grad} P + \operatorname{div}(\hat{\tau})$

- energy balance equation $\dfrac{\partial (\rho\varepsilon)}{\partial t} + \operatorname{div}(\rho\varepsilon \mathbf{V}) = -P \operatorname{div} \mathbf{V} - \operatorname{div} \mathbf{Q} - G_{\mathrm{Rad}} + \Phi$

viscosity forces: $(\hat{\tau}) = \mu \Delta \mathbf{V} + \left(\xi + \dfrac{\mu}{3}\right) \operatorname{grad}(\operatorname{div} \mathbf{V})$

viscous dissipation of energy: $\Phi = \sum\limits_{i,k} \dfrac{\mu}{2} \left(\dfrac{\partial V_i}{\partial x_k} + \dfrac{\partial V_k}{\partial x_i} \right)^2 + \left(\xi - \dfrac{2}{3}\mu \right) (\operatorname{div} \mathbf{V})^2$

ξ, μ — viscosity coefficients

Common notations for physical values is used here. The full internal energy ε includes the energy of vibration excitement, dissociation and ionization. The last equation is taken in a one-temperature approximation and includes radiation losses. We suppose that the flow exists under LTE (local thermodynamic equilibrium) condition and energy consumption for vibration excitement, dissociation, and ionization is accounted by the use of tabulated internal energy dependence upon density and temperature.

The solution of the RGD system is done by use of unstructured triangular mesh. The main advantage of unstructured meshes is the ease of boundary fitting and refinement procedures implementation. We utilize the node-centered (nonstaggered) representation of calculated values. The technique of finite volumes is used for approximation of the governing system. In the present program version the finite volumes are formed by modified Voronoi diagrams. The triangular mesh in the computational domain and a zoomed fragments of the initial triangular grid and the finite volumes near the body head are shown below.

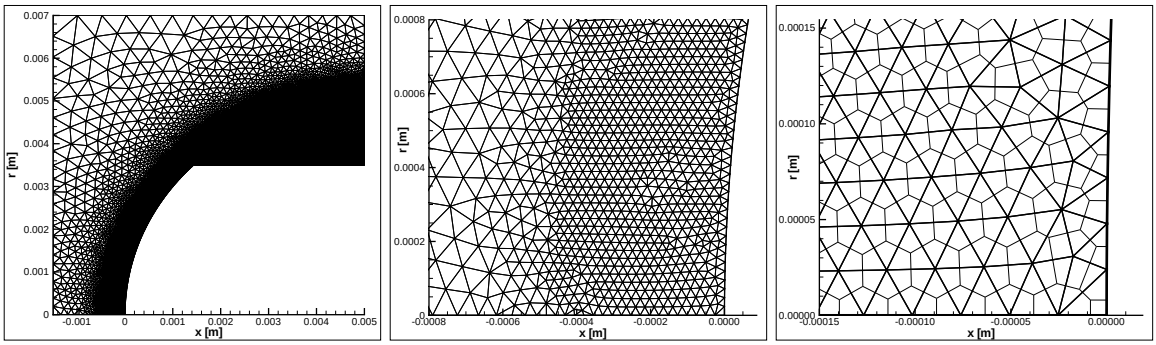

Figure 1. The triangular mesh in the computational domain.

A splitting scheme is applied to the governing system with the subsets of equations describing different physical processes being solved in sequence by appropriate program modules. The GD system is solved by the generalized TVD Lax-Friedrichs scheme which was developed especially for the unstructured mesh applications [4]. For the case of a regular triangulation this scheme ensures the second order approximation to spatial derivatives (the third order is possible with a special choice of the antidiffusion limiters). The time integration is explicit, the second approximation order is reached due to the predictor - corrector procedure. The time step is restricted by the Courant criterion. For the solution of parabolic equations describing the conductive heat transfer, we developed the new finite-volume schemes constructed by analogy with mixed finite-element method.

Radiative energy transfer is described by the equation for spectral radiation intensity. Practical calculations are done via multigroup spectral approximation. We solve the radiative transport equation by means of semi-analytical characteristic algorithm. The analytical solution along the characteristic direction is constructed by means of the backward-forward angular approximation to the photon distribution function [2], [3]. The two-group angular splitting gives an analytical expression for radiation intensity dependent on opacity and emissivity coefficients. The radiation-matter energy exchange is taken into account via a radiative flux divergence, which is incorporated into the energy balance as a source function.

Transport equation for quasistationary radiation field in cylindrical geometry:

$$\sin\theta\left(\cos\varphi\frac{\partial I_\omega}{\partial r}+\frac{\sin\varphi}{r}\frac{\partial I_\omega}{\partial\varphi}\right)+\cos\theta\frac{\partial I_\omega}{\partial z}=-\aleph_\omega I_\omega+j_\omega$$

A set of equations for the forward/backward intensity functions $I^{f/b}$:

$$\frac{\cos\theta_{n+1}-\cos\theta_n}{\Delta\theta_n}\left(\frac{\partial I^b_{n+1/2}}{\partial r}+\frac{I^b_{n+1/2}}{r}\right)+\frac{\sin\theta_{n+1}-\sin\theta_n}{\Delta\theta_n}\frac{\partial I^b_{n+1/2}}{\partial z}=-\aleph I^b_{n+1/2}+j$$

$$\frac{\cos\theta_n-\cos\theta_{n+1}}{\Delta\theta_n}\left(\frac{\partial I^f_{n+1/2}}{\partial r}+\frac{I^f_{n+1/2}}{r}\right)+\frac{\sin\theta_{n+1}-\sin\theta_n}{\Delta\theta_n}\frac{\partial I^f_{n+1/2}}{\partial z}=-\aleph I^f_{n+1/2}+j$$

The radiation energy density

$$U=\frac{\pi}{c}\sum_{n=1}^{N}\left(I^f_{n+1/2}+I^b_{n+1/2}\right)(\cos\theta_n-\cos\theta_{n+1})$$

The forward/backward intensities along a ray in the direction $\theta_{n+1/2}$

$$I^{f/b}=(I^{f/b}_{i,j+1}-I^{eq}_{i,j})\exp(-\kappa_{i,j}\xi_{i,j})+I^{eq}_{i,j}$$

For the purpose of the radiation energy transport calculation a special grid of characteristics is constructed in the computational area. This grid is formed by a number of sets (families) of parallel right lines and is further referred to as the grid of rays. Each set of parallel lines is characterized by the angle of inclination to coordinate axes and spatial density of rays. The grid of rays introduces some discretization of the computational area in the plane (r,z) and also with respect to the angle θ, $(0<\theta<\pi)$, which is required for numerical integration of the radiation transport equation according to the described above model. The grid of rays is superimposed on the initial computational grid intended for gas dynamics and heat transfer computations. A fragment of the grid of rays (12 angle sectors) is shown at the figure.

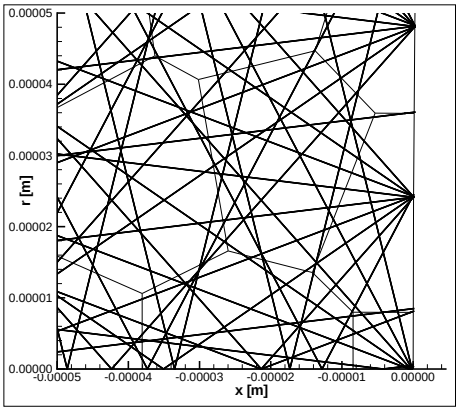

Figure 2. A fragment of the grid of rays.

2. Thermodynamic and optical properties of the air

For practical applications the datatables of material properties as to thermodynamics, ionisation, opacities and emissivities are used. A wide-range equation of state was constructed for the air composition: $78.12\% - N_2$, $20.95\% - O_2$, $0.93\% - Ar$ (hereinafter - the air). The effective ranges of the thermodynamic functions values in the developed equation of state are the following:

for the temperature: 200 to $1.16 \cdot 10^5$ K;

for the density: 10^{-3} to 18 g/m^3;

for the pressure: $5.7 \cdot 10^{-8}$ to 3.7 GPa;

for the specific internal energy: $1.4 \cdot 10^{-1}$ to $8.3 \cdot 10^4$ kJ/g.

The model of plasma imperfection with the classic Coulomb correction Debye-Hukkel in big canonical ensemble (BDH) was applied in the computations. Generation and dissociation of two- and three- atom molecules were accounted as well as adhesion of electrons at the atoms and molecules. Statistical sums for the atoms and molecules were calculated using up-to-date statistical sums truncation models. Up to 10-15 electron states were considered in calculation of the full statistical sums. Microfield truncation formfactor was employed for statistical sums calculation for atoms and ions. The molecules N_2, O_2, NO, their first positive ions, negative ions O_2, NO, O, and all the atomic positive ions up to their maximum charge number were considered in the computations. (See the figure a.)

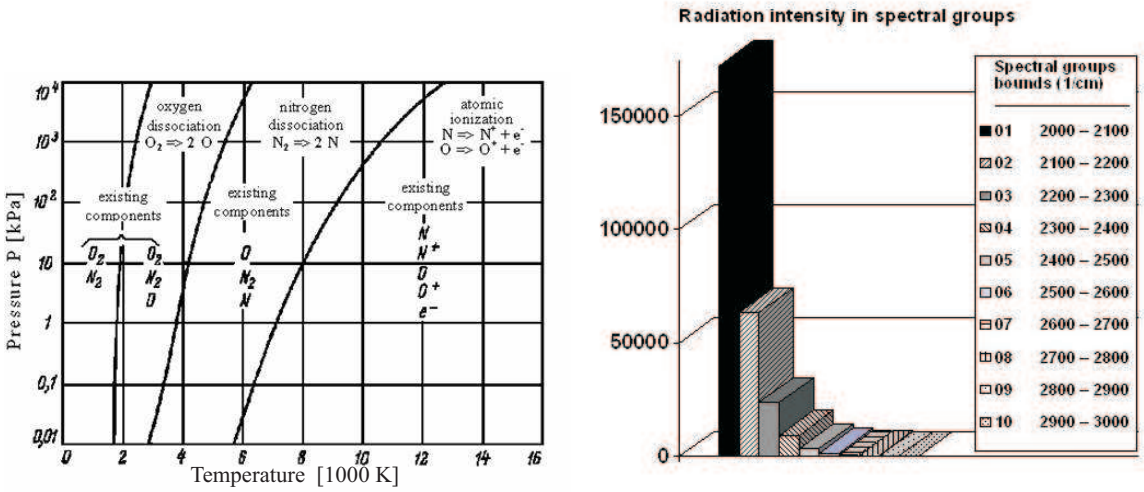

Figure 3. a) Dissociation bounds of the air components. b) Radiation in spectral intervals.

The spectral absorption coefficients were calculated for 20 spectral groups (Plank and Rosseland averaging as well as that with a unit weight factor) in the range of temperature T from 200 to $5.5 \cdot 10^4$ K and the range of relative density ρ from 10^{-3} to 10. The opacities were calculated for the wavenumber band from 2000 cm^{-1} to 500000 cm^{-1} split uniformly by 250 groups. Due to the required temperature range the mathematical modelling of the air composition optical properties was accomplished here by the use of semiempirical model of continuous spectrum. The calculations were done taking into account the influence of spectral lines. Then 20 group spectral model of the high-temperature air composition opacity coefficients was constructed for the radiation gasdynamics

tasks, the boundaries of the averaging ranges being chosen purposely to provide the best description of the radiation energy transport for T near $20 \cdot 10^3$ K. The Plank and Rosseland averaging as well as that with a unit weight factor was carried out. Noteworthy that the maximal deviation in integral Plank absorbtion coefficient between our calculated value and those obtained by another technique independently was only 4%.

First the 20 spectral groups bounds were chosen in the range 2000 - 500000 cm^{-1}. But the numerical experiments showed that the entire radiation is concentrated in the first group (2000 - 4000 cm^{-1}). Then a new set of spectral groups was introduced to be used in practical computations. The above diagram (the figure b) demonstrates the radiation intensity distribution in the first 10 of these groups. The radiation in the rest 10 groups is almost negligible. Radiative energy flux was evaluated at the body head surface.

3. Data structures and parallel implementation

A universal program tools were developed convenient for input and acquisition of geometrical/physical data as well as for storage and treatment of a discrete computational model. Cellular model is used for both the computational domain and the meshes described as geometric complexes. A formalized description of geometric and topological properties of meshes is thus provided. Topological complexes of various dimensionality are suitable for representation of irregular continuum as well as discrete structures. 3D geometric complex includes: 0-order elements (nodes), 1-order elements (edges), 2-order elements (faces), and 3-order elements (cells). The boundary of each element is formed by the elements of lower order. Topology is described by relations between the elements. Two types of relations are used: incidence relations (between elements of different dimensions) and adjacency relations (between elements of the same dimension). Only a few base incidence relations are stored permanently and other relations are calculated every time we need them. Dynamic topology changes are supported. Each element is identified by its number. Having the number of an element, it is possible to find all the data assigned to this element. Special methods were developed that allow to implement for all data structures appropriate changes caused by variations in elements numeration (e.g. adding or removing the elements while grid construction or refinement).

This geometric data treatment technique is especially effective for unstructured grids, but may be applied for regular grids as well. It is also useful for handling subdomains processed by a distributed computer system.

The developed explicit difference scheme allows quite natural parallel implementation for distributed computer systems. Each processing node is associated with a section of the triangular computational grid (a subdomain). Each processor carries out the computations only inside this subdomain. Subdomains cover the entire computational grid and may have common nodes only at the boundaries. The data exchange between subdomains is organized through the "margins". We called so the layers of grid elements belonging to the neighboring subdomains. In that way some elements of a subdomain are included in the "margins" of the neighboring subdomains. Any data from a margin node are to be retrieved via high-speed network from the processor where this node is stored as an element of the related subdomain.

Numerical experiments showed that it is necessary to pay a special attention to the proper domain decomposition in order to minimize the problem time. The load of the processors should be well balanced. Otherwise downtime is inevitable when an underloaded processor finishes a step of calculations and is waiting until the neighboring overloaded processors will be able to provide the requested data. We use MPI for distributed computations and ParMetis for mesh partition.

Another important factor is the avoidance of collisions, i.e. the proper time balancing of the net-

work channel loading. The processors should not request the network data exchange simultaneously with the network being then idle for a relative long time. A downtime may occur because of insufficient network throughput thus increasing the overall computation time notably. This problem is fixed by a special order of calculations in the internal and boundary nodes in subdomains.

Implementation of complex physical models incorporating multi-scaled and essentially non-local processes requires more than one grid structure. For instance, an additional grid of rays (characteristics) is necessary for the simulation of radiative energy transfer by the method of characteristics. As a rule, the number of elements (and therefore the resources consumption) of these grids are comparable. In this case it is reasonable to arrange distributed computing involving not only domain decomposition but the splitting of the physical processes as well. That means that a special group of processors may be provided for the radiation transfer simulation. The multigroup model allows separated computations for each spectral group. Thus the spectral groups may be distributed for a several processors. It is important that an intensive non-local data exchange exists between the different grid structures. When the transport equation is solved along the characteristics each of them crosses several subdomains and both the internal and boundary cells are crossed. Thus additional conditions are introduced into the interprocessor communications balancing problem - we have to optimize the rays distribution over the triangular grid partition. Rays crossing the basic grid subdomains are schematically shown at the diagram.

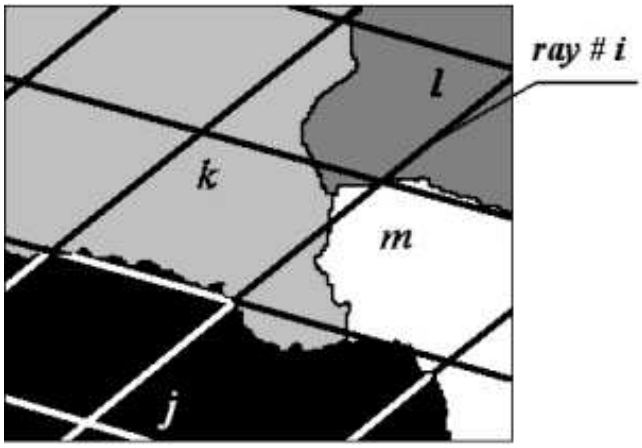

Figure 4. The grid of rays over domain partition.

The basic triangular grid is partitioned to N domains located at N processors ($N = 16$ in our case). We are to distribute M rays (grid of characteristics) over the same processors ($M = 3845$). Each ray is divided into segments, associated with the basic grid cells (control volumes). Each ray is processed individually. The computations are carried out along a ray, and each segment utilizes the calculated data from the related cell (because the optical properties at a segment are dependent upon the temperature and the density in the cell). That means that if the ray $\#i$ is processed by the processor j and the cells involved are located in the domains j, k, l, m, only the data from the domain j cells may be acquired directly, and those from the domains k, l, m require communications between the processors $j-k$, $j-l$, $j-m$. The number of ray segments varies significantly. Some rays may include only two segments and some a hundred or more. A lot of rays cross several domains. That's why an optimization of ray distribution is important.

Boolean linear programming problem statement.

Unknown variables: $x_{ij} = \begin{cases} 1 & \text{if the ray } \#i \text{ is at the processor } j \\ 0 & \text{otherwise} \end{cases}$

Limitations: each ray should be included in the partition exactly once: $\forall i \sum\limits_{i} x_{ij} = 1$.

Criterion function 1. The number of interprocessor communications.

$$F_1 = \sum_i \sum_j a_{ij}(1-x_{ij}) \to min$$

Weight factor a_{ij} is the number of ray $\#i$ segments located in the domain j. It is the number of segments acquiring the information from the processor j. In particular $a_{ij} = 0$ if the ray $\#i$ does not cross the domain j.

Criterion function 2. The processor load balance.

$$F_2 = \sum_k \sum_l (\varphi_k - \varphi_l)^2 \to min$$

Here $\varphi_j = \sum\limits_i b_i x_{ij}$ is the number of rays segments processed by the processor j.

$b_i = \sum\limits_j a_{ij}$ is the total number of ray $\#i$ segments.

The aggregate criterion function: $F = \alpha F_1 + \beta F_2$.

The factors α and β depend upon the estimations of the interprocessor communication time (α) and the ray processing time (β).

For practical computations a heuristic optimization algorithm was applied.

4. Numerical results

The constructed algorithms were examined in numerical experiments related to the problem of satellite re-entry studies.

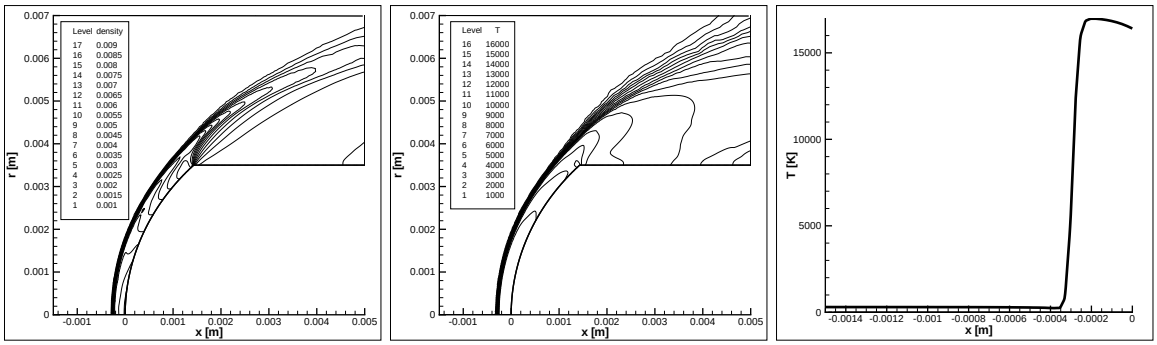

Figure 5. Calculated density and temperature distribution.

To verify the accuracy of the presented approaches the calculations was made for the flow around the spherically nosed cylinder with 0.5 cm radius and 0.7 cm cylinder diameter. In the present study the shock layer flow over this model at the free-stream density $5.5 \cdot 10^{-4}$ kg/m^3 and the temperature

300K was studied for two different values of the free-stream velocity 13.4 km/s and 16 km/s. We suppose the following boundary conditions: a slip conditions at the wall, a zeroth-order extrapolation at the outflow boundary, a symmetry condition in the symmetry plane, and the free-stream condition at the inflow boundary. For the radiation processes the far-field is assumed be a black body having a temperature 300 K. The wall is assumed to be a black body at 3000 K.

The simulations showed an excellent resolution of flow structures and high performance capability of the developed code. The above figures illustrate density and temperature distribution near the blunt body and the temperature distribution along the stagnation line for the case of the free-stream velocity of 16 km/s.

The numerical results are in good agreement with experimental data given in [5].

5. Conclusions

1. The numerical simulation is an important tool for re-entry studies as it allows to circumvent the problem of absence of "scaling" parameters at presence of chemical transformations, which complicates theoretical studies of hypersonic flows.

2. The flowfield around a re-entry satellite can be simulated quite well by means of numerical technology based on unstructured grids locally refined for precise treatment of shocks and boundary layers. The corresponding results are in good agreement with experimental observations as well as theoretical predictions and previous numerical studies.

3. For the studied problems the radiative transfer exerts rather small influence on the whole energy balance in the near-body region. Taking into account the wall evaporation by means of introducing some amounts of gaseous carbon into the boundary layer has no important influence on the radiative properties of the flow. The energy balance under the assumed flight conditions depends mainly on dissociation-recombination in the air past the head shock wave and in the boundary layer.

4. Further investigations of the re-entry problem require taking into consideration the nonequilibrium chemical transformations in the shock.

5. To estimate more comprehensively the influence of radiative transfer it is necessary to simulate the re-entry flow for various flight conditions, i.e. for various altitudes, free-stream Mach number and at various attack angles.

6. For the last item the application of 3D simulation tools is necessary.

References

[1] L.D.Landau and E.M.Livshits. A course in theoretical physics. Vol VI "Hydrodynamics". Moscow, "Fizmatlit", 1986.

[2] R.Siegel, J. R.Howell. Thermal radiation heat transfer. Tokyo, McGraw-Hill, 1972.

[3] B.N.Chtverushkin. Mathematical modeling in radiative gasdymnamic problems. Moscow, Nauka publ., 1985.

[4] V.A.Gasilov and S.V.D'yachenko. Quasimonotonous 2D MHD scheme for unstructured meshes. Mathematical Modeling: modern methods and applications. Moscow, Janus-K, 2004, pp.108-125.

[5] Sakai T., Tsuru T. and Sawada K., Computation of Hypersonic Radiating Flowfield over a Blunt Body, Journal of Thermophysics and Heat Transfer, Vol. 15, N 1, 91-98, 2001.